Military Technical College
Kobry El-Kobbah,
Cairo, Egypt.

17th International Conference on Applied Mechanics and Mechanical Engineering.

NUMERICAL STUDY ON WIND TURBINE WAKES UNDER THERMALLY-STRATIFIED CONDITIONS

M. R. Abuhegazy[1], A. M. AbdelSalam[2], I. M. Sakr[2] and W. A. El-Askary[3]

ABSTRACT

In the present work, the wake behavior of wind turbines operating under thermally-stratified atmospheric boundary layer (ABL) is numerically investigated. The steady state three dimensional Reynolds-Averaged Navier–Stokes (RANS) equations, combined with actuator disk approach, are used in the simulation. The standard k-ε turbulence model as well as two modified models namely Crespo model and El kasmi model are adopted. Two different methods are used and compared, to represent the atmospheric stratification conditions. In the first method, the energy equation is considered along with mass, momentum, and turbulence model equations. The stratification in the second method is modeled by means of an additional buoyancy production or dissipation term, which is added to the equation of the turbulent kinetic energy, instead of solving the energy equation. The results obtained from both methods show reasonable agreement with the experimental data available from the literature.

KEYWORDS

Wind turbine wakes; Actuator disk; Atmospheric thermal stratification; Atmospheric boundary layer; RANS, k-ε model

[1] Demonstrator, Dept. of Mech. Power Eng., Menoufia University, Shebin El-Kom, Egypt.
[2] Assistant Professor, Dept. of Mech. Power Eng., Menoufia University, Shebin El-Kom, Egypt.
[3] Professor, Dept. of Mech. Power Eng., Menoufia University, Shebin El-Kom, Egypt

INTRODUCTION

Wind turbine wakes have attracted a lot of attention of research community in recent years because of their effect on power production of wind farms. These wakes are characterized by a reduction of wind speed which in turn reduces the available wind power and an increase of turbulence levels that generate fatigue loads on downstream wind turbines. As a result, the investigation of wind turbine wakes becomes very important to study their influence on the performance of the other downstream turbines so as to install as many as possible wind machines within a limited area and to reduce maintenance cost of wind farm due to dynamic loads.

Wind turbines operate in the lowest region of the atmospheric boundary layer (ABL). Therefore, the evolution and recovery of wind turbine wakes are strongly affected not only by the turbine characteristics and complexity of terrain, but also, by the ambient wind speed and turbulence levels related to different thermal stratifications of ABL. A proper modeling of all these factors becomes mandatory for detailed understanding and accurate prediction of wind turbine wakes and their effects on the performance of the whole wind farm.

According to the thermal conditions, the atmospheric boundary layer can be classified into three types, which are neutral (NBL), stable (SBL), and unstable or convective (CBL). In NBL, the mean potential temperature is approximately constant with height, so that the generated turbulence is mainly due to the ground surface. It is observed only during windy weather with clouds. In SBL, the ground surface is colder than the ambient air, therefore, the generated turbulence by shear is suppressed by negative buoyancy resulted from vertical downward heat flux. This atmospheric condition usually occurs at night time. The third type, CBL, occurs during day time when the ground surface is warmer than ambient air. The vertical upward heat flux generates a positive buoyancy which in turn enhances the ambient turbulence. It is observed that, the turbulence level varies in descending order of magnitude in CBL, NBL and SBL respectively.

Full-scale field measurements as well as wind tunnel experiments of small-scaled models of wind turbines showed significant effect of thermal stratification on wind power production and structure of wind-turbine wakes, as reported in [1-5]. Baker and Walker [6] used kite anemometry to measure wake deficits of two MOD-2, 2.5 *MW*, 91*m* diameter wind turbines. The measurements were obtained at different ambient turbulence levels under stable condition at Goodnoe Hills, Washington. The results indicated that the wake velocity deficits 9 diameters downwind are on the order of 15 – 18%, while these deficits decrease to less than 10% under more turbulent night-time flow. Magnusson and Smedman [7] investigated the influence of atmospheric stability on the wake structure of wind turbines operating at Alsvik wind farm. Their results showed that the different atmospheric stratifications affect the velocity deficit and the largest velocity deficit was observed under stable condition. Iungo and Porté-Agel [8] measured turbulence intensity and wind velocity field of the wake produced by a 2-*MW* Enercon E-70 wind turbine, using Doppler wind lidars. The measurements were carried out at different atmospheric stratification conditions. It was observed that there is a significant reduction of turbulence activity within the atmospheric surface layer moving from CBL to NBL regimes, which in turn causes the wake to recover faster under convective regime compared with neutral one. Similar behavior of wake recovery was observed during wind tunnel measurements of Zhang et al. [4]. They used stereoscopic

particle image velocimetry (S-PIV) and triple-wire anemometry to study the effects of CBL on velocity deficits, turbulence intensities and tip vortices of the wakes of small scale wind turbine. Also, Hancock and Pascheke [5] carried out a wake measurements in the EnFlo stratified-flow wind tunnel operating under neutral and stable atmospheric boundary layer. Their measured data showed that the wake recovery is slower in SBL compared with NBL condition. This behavior is qualitatively consistent with the field measurements reported by Magnusson and Smedman [9].

Besides field measurements and wind tunnel experiments of wind turbine wakes, analytical and numerical models have also addressed the effect of atmospheric stability on wind turbine wake behavior, see [10-16]. Bastankhah and Porté-Agel [17] proposed a new analytical model based on self-similar Gaussian wake velocity distribution to predict the velocity deficit downstream of wind turbines operating under neutrally-stratified flow condition. The model was tested against wind tunnel measurements of Chamorro and Porté-Agel [3] and Large-Eddy Simulation (LES) data for real-scale wind turbine wakes of Wu and Porté-Agel [18-19]. The results showed an acceptable agreement with the aforementioned test cases. However, Bastankhah and Porté-Agel [17] recommended performing more research to consider the effect of inflow conditions on the wake growth rate. Recently, Abkar and Porté-Agel [20] used LES frame work combined with actuator disk model with rotation to investigate the effect of atmospheric thermal stability on wind turbine wakes produced by Vestas V80-2*MW* wind turbine. Their results indicated that, the spatial distribution of the wake characteristics is strongly affected by the different atmospheric stratifications. In particular, the wake recovers faster under convective conditions compared with the other two conditions due to higher turbulence level of incoming wind in CBL. In addition, they used the results to calibrate the model of Bastankhah and Porté-Agel [17] and proposed a developed one assuming an elliptical (instead of axisymmetric) Gaussian distribution for the wake deficit, taking into account the different thermal stratification of ABL.

To the best of our knowledge, simulation of the wind turbine wakes under thermally-stratified atmosphere using Reynolds-Averaged Navier–Stokes (RANS) technique is not well documented in the literature. The present paper aims to test this technique in order to investigate the wake behavior at different ambient stability conditions. Two different methods, described in the next section, which are direct and indirect methods, are adopted and compared for representing the buoyancy effect produced by ambient stratification. The standard k-ε model of Launder and Spalding [21] and another two modified models of Crespo et al. [22] and El Kasmi and Masson [11] are used for turbulence modulation. The two modified models will be referred to hereafter as Crespo model and El Kasmi model. The Monin-Obukhov similarity theory is used for describing the atmospheric conditions under the influence of heat transfer, see Arya [23].

MATHEMATICAL MODELING

In the present work, the numerical simulation of wind turbine wakes under different thermally-stratified conditions of ABL is based on RANS equations. The flow is considered as steady, incompressible and ideal gas. Also, the buoyancy effect due to atmospheric thermal stratifications is taken into account. Based on these assumptions,

the continuity, momentum and energy equations according to Alinot and Masson [24] are solved.

The continuity and momentum equations are given by,

$$\frac{\partial \rho u_j}{\partial x_j} = 0 \tag{1}$$

$$\frac{\partial \rho u_i u_j}{\partial x_j} = -\frac{\partial p}{\partial x_i} + \frac{\partial \tau_{ij}}{\partial x_j} + S_m \tag{2}$$

where, $S_m = \rho\, \mathrm{g}_i$ is the momentum added source term to represent the gravity force and τ_{ij} is the Reynolds stress tensor of eddy viscosity model that is given by:

$$\tau_{ij} = \mu_e\left(\frac{\partial u_i}{\partial x_j} + \frac{\partial u_j}{\partial x_i}\right) \tag{3}$$

where, $\mu_e = \mu + \mu_t$ is the effective viscosity and μ_t is the turbulent viscosity, calculated from the adopted turbulence closure.

The energy equation is written as:

$$\frac{\partial}{\partial x_j}\rho c_p u_i T = \frac{\partial}{\partial x_j}\left[u_j \tau_{ij} + \frac{c_p \mu_t}{\sigma_T}\left(\frac{\partial T}{\partial x_i} - \Gamma\right)\right] + S_E \tag{4}$$

where, $S_E = \rho u_i \mathrm{g}_i$ is the added source term to the energy equation to account for gravity effect and $\Gamma = \mathrm{g}_i / c_p$ is the dry adiabatic laps rate added to the energy equation in order to reformulate the temperature gradients based on potential temperature θ that is related to the temperature by

$$\frac{\partial \theta}{\partial z} = \frac{\theta}{T}\left(\frac{\partial T}{\partial z} + \Gamma\right) \cong \frac{\partial T}{\partial z} + \Gamma \tag{5}$$

In the direct modeling of atmospheric stratification, the complete set of continuity, momentum and energy equations are considered. However, in the indirect method, instead of solving the energy equation, the atmospheric stratifications (SBL and CBL) are represented using additional buoyancy production and dissipation source terms G and G_ε which are added to the turbulent kinetic energy equation and its dissipation rate equation, respectively as reported by Stull [25]. These terms are defined as:

$$G = -\mu_t\left(\frac{\partial u}{\partial z}\right)^2 \frac{Ri}{\mathrm{f}_m} \quad \text{and} \quad G_\varepsilon = G\frac{\varepsilon}{k} \tag{6}$$

where,

$$\mathrm{f}_m = 1 + 5\zeta \;; \quad \zeta = z/L \quad \text{and} \quad Ri = \begin{cases} \zeta \frac{0.74 + 4.7\zeta}{(1+4.7\zeta)^2} & L > 0 \\ \zeta & L < 0 \end{cases} \tag{7}$$

where, Ri is the Richardson number, ζ is the stability parameter, z is the vertical distance from ground surface and L is the Monin-Obukhov length.

Modeling of Wind Turbine

The actuator disk approach is used to represent the effect the turbine rotor on the flow. The rotor is simulated as a momentum sink to be applied on the surface of the actuator disk according to:

$$F = 0.5\rho C_T A U_{hub}^2 \tag{8}$$

where, *A* is the surface area of the turbine rotor, and C_T is the thrust coefficient that is obtained from the thrust coefficient curves against wind velocity for the modeled turbines at the given hub height velocity u_{hub}. The selected C_T is assumed to be constant across the whole actuator disk. As a result, the calculated thrust force is uniformly distributed over the disk. The assumption of constant C_T is used because the non-uniform calculation of C_T over the rotor disk would require the coupling of the Navier–Stokes solver with a Blade Element Momentum (BEM) theory solver. Also, it requires detailed data of the blade geometry and the lift coefficient (C_L) and the drag coefficient (C_D) distributions of the airfoils along the span of the blades, which are usually not available.

Turbulence Modeling

The widely used two-equation standard k-ε turbulence model by Launder and Spalding [21] is employed. In addition, two modified k-ε models of Crespo et al. [22] and El Kasmi and Masson [11] are also used trying to improve the prediction of the wake behavior.

In the standard k-ε model, the transport equation for turbulent kinetic energy (k) is given as:

$$\frac{\partial}{\partial x_j}\rho k u_j = \frac{\partial}{\partial x_j}\left[\left(\mu + \frac{\mu_t}{\sigma_k}\right)\frac{\partial k}{\partial x_j}\right] + P_t + G_b - \rho\varepsilon \tag{9}$$

where, P_t is the production term of turbulent kinetic energy due to shear, which is calculated from:

$$P_t = \mu_t \left(\frac{\partial u_i}{\partial x_j} + \frac{\partial u_j}{\partial x_i}\right)\frac{\partial u_i}{\partial x_j} \tag{10}$$

and G_b is the generation of turbulent kinetic energy due to buoyancy that is given by:

$$G_b = \beta\, \mathrm{g}_i \frac{\mu_t}{\sigma_T}\left(\frac{\partial T}{\partial x_i} - \frac{g_i}{c_p}\right) \tag{11}$$

Here, β is the air thermal volumetric expansion coefficient. It is defined as:

$$\beta = -\frac{1}{\rho}\frac{\partial \rho}{\partial T} = \frac{1}{T} \tag{12}$$

The dissipation rate equation (ε) is written as:

$$\frac{\partial}{\partial x_j}\rho\varepsilon u_j = \frac{\partial}{\partial x_j}\left[\left(\mu + \frac{\mu_t}{\sigma_\varepsilon}\right)\frac{\partial \varepsilon}{\partial x_j}\right] + C_{1\varepsilon}\frac{\varepsilon}{k}(P_t + C_{3\varepsilon}G_b) - \rho C_{2\varepsilon}\frac{\varepsilon^2}{k} \tag{13}$$

Once the k and ε equations are solved, the turbulent viscosity is then calculated from:

$$\mu_t = \rho C_\mu \frac{k^2}{\varepsilon} \tag{14}$$

Note that, in the original model proposed by Jones and Launder [26], $G_b = 0$ and the values of the model constants are:

$$\sigma_k = 1;\ \ \sigma_\varepsilon = 1.3\ ;\ \ C_{1\varepsilon} = 1.44\ \ ;\ \ C_{2\varepsilon} = 1.92\ ;\ \ C_\mu = 0.09$$

In ANSYS FLUENT 15, $C_{3\varepsilon}$ is not specified, but is instead calculated according to the following relation $C_{3\varepsilon} = \ tanh|v/u|$ as mentioned in FLUENT 15 theory guide [27].

In Crespo model, it was considered that there is a decrease in the turbulence decay ratio due to the atmospheric turbulence so that, the authors in [22] proposed a new model constants consistent with ABL flow which are:

$$\sigma_k = 1;\ \ \sigma_\varepsilon = 1.3\ ;\ \ C_{1\varepsilon} = 1.176\ \ ;\ \ C_{2\varepsilon} = 1.92\ ;\ \ C_\mu = 0.033$$

For El Kasmi model, an additional production term P_ε first proposed by Chen and Kim [28] is added to the ε-equation to represent the energy transfer rate from large-scale turbulence to small-scale turbulence (energy cascade) in the near wake region. Consequently, it is added only in a cylindrical volume upstream and downstream the turbine of approximately 0.25*D* (*D* is the turbine rotor diameter) as proposed by El Kasmi and Masson [11]

$$P_\varepsilon = C_{4\varepsilon}\frac{P_t^2}{\rho k} \tag{15}$$

The model constants of Crespo et al. [22] are used for El Kasmi model. In addition, the constant $C_{4\varepsilon}$ is taken to be 0.37 in El Kasmi model instead of 0.25 as suggested by Chen and Kim [28].

DESCRIPTION OF ABL FLOW

In common, the Monin-Obukhov similarity theory is the suitable framework for describing ABL flow under the different thermal stratifications. In this theory, the degree of stability of atmosphere is defined based on Monin-Obukhov length L. Its magnitude $|L|$ is define as the vertical height where G_b is comparable with P_t, see Alinot and Masson [24] and Apsley and Castro [29]. The Monin-Obukhov length is given by:

$$L = \frac{u_*^2 T_w}{\kappa g T_*} \tag{16}$$

where, $u_* = \sqrt{\tau_w/\rho}$ is the friction velocity, $T_* = -\dot{q}_w/\rho c_p u_*$ is the scaling temperature, T_w is the ground surface temperature, κ is the von Karman constant ($\kappa = 0.41$), g is the gravitational acceleration, τ_w is the surface shear stress and $\dot{q}_w$ is the surface heat flux.

According to the Monin-Obukhov similarity theory, the vertical distribution of ABL flow variables for stable ($L > 0$) and convective ($L < 0$) conditions are given by Alinot and Masson [24] as:

$$u(z) = \begin{cases} \frac{u_*}{\kappa}\left[ln\left(\frac{z+z_0}{z_0}\right) + \phi_m\left(\frac{z}{L}\right) - 1\right] & L > 0 \\ \frac{u_*}{\kappa}\left[ln\left(\frac{z+z_0}{z_0}\right) + ln\left(\frac{8\phi_m^4\left(\frac{z}{L}\right)}{\left(\phi_m\left(\frac{z}{L}\right)+1\right)^2\left(\phi_m^2\left(\frac{z}{L}\right)+1\right)}\right) - \frac{\pi}{2} + 2\,tan^{-1}\left(\frac{1}{\phi_m\left(\frac{z}{L}\right)}\right)\right] & L < 0 \end{cases} \tag{17}$$

$$T(z) - T_w = \begin{cases} \frac{T_*}{\kappa}\left[ln\left(\frac{z+z_0}{z_0}\right) + \phi_m\left(\frac{z}{L}\right) - 1\right] - \frac{g}{c_p}(z - z_0) & L > 0 \\ \frac{T_*}{\kappa}\left[ln\left(\frac{z+z_0}{z_0}\right) - 2\,ln\left[\frac{1}{2}\left(1 + \phi_m^{-2}\left(\frac{z}{L}\right)\right)\right]\right] - \frac{g}{c_p}(z - z_0) & L < 0 \end{cases} \tag{18}$$

$$k(z) = \frac{u_*^2}{\sqrt{C_\mu}}\left[\frac{\phi_\varepsilon\left(\frac{z}{L}\right)}{\phi_m\left(\frac{z}{L}\right)}\right]^{\frac{1}{2}} \tag{19}$$

$$\varepsilon(z) = \frac{u_*^3}{\kappa(z+z_0)}\,\phi_\varepsilon\left(\frac{z}{L}\right) \tag{20}$$

where,

$$\phi_m\left(\frac{z}{L}\right) = \begin{cases} 1 + 5\frac{z}{L} & L > 0 \\ \left(1 - 16\frac{z}{L}\right)^{-\frac{1}{4}} & L < 0 \end{cases} \quad \text{and} \quad \phi_\varepsilon\left(\frac{z}{L}\right) = \begin{cases} 1 + 4\frac{z}{L} & L > 0 \\ 1 - \frac{z}{L} & L < 0 \end{cases} \tag{21}$$

where, z_0 is the aerodynamic roughness length and ϕ_m and ϕ_ε are dimensionless wind shears.

COMPUTATIONAL DOMAIN AND GRID GENERATION

The computational domain shown in Fig.1 is extended 30*D* in the stream wise direction

(x- co-ordinate), 8*D* in the lateral direction (y- co-ordinate) and 6*D* in the vertical direction (z- co-ordinate). Howell et al. [30], reported that, the blockage ratios below the range of 6 – 7.5 % have a negligible effect on the flow. Using the aforementioned dimensions of the computational domain, the blockage ratio in the present simulation is about 1.636 % which is in the acceptable range. The simulated actuator disk is positioned 5*D* downstream of the inlet boundary, in the middle distance between the two lateral sides of the domain.

The three-dimensional CAD model of the computational domain is completed using SolidWorks program then, it is imported to ANSYS ICEM program which is used for generating the computational grid. A three-dimensional unstructured mesh of suitable grid sizes is constructed. Fig. 2 shows the generated grid, in which the mesh element sizes are controlled to obtain fine girds around and downstream of the actuator disk. This is to resolve the strong gradients in the wake region and to account for wake expansion downstream of the rotor disk. Fine prism elements with an expansion factor of 1.15 are used near the ground wall. Accordingly, the dimensionless wall distance (y^+) is found to be in the range of 40-90, which is suitable for the adopted near wall functions. The total number of cell elements is found to be 1.2 million cells.

BOUNDARY CONDITIONS AND SOLUTION METHODOLOGY

The inlet boundary is a plane located 5*D* upstream of the rotor disk as shown in Fig.1. At this boundary, the velocity inlet boundary condition (BC) is chosen, in which the change of axial velocity component with height is prescribed using Eq. (17), while the other inlet velocity components are set to be zero. Also, the vertical distribution of temperature is calculated from Eq. (18) and the turbulent quantities k and ε are defined by Eq. (19) and Eq. (20), respectively. It is observed that there is a negative pressure gradient with vertical direction due to the buoyancy effect. Hence, at the outlet boundary, the pressure outlet BC is used, in which the vertical distribution of static pressure is implemented as a profile calculated from inlet instead of considering zero value relative to the atmospheric pressure in order to get rid of the reverse flow from outlet boundary. In addition, the temperature is expected to reach developing state so that, the outlet temperature distribution is set just like the inlet boundary. The lateral sides are far enough from the rotor disk. Thus, they are treated using symmetry BC, in which the normal gradient of all flow variables across this boundary are neglected. For the upper plane, the upstream flow properties are maintained constant. The near wall treatment of Parente et al. [31] is implemented in the near ground region, to calculate velocity, turbulent kinetic energy and turbulent dissipation rate consistent with the inlet turbulence quantities. Furthermore, the ground is maintained at constant temperature. The FLUENT fan model is adopted for describing the actuator disk. In this model, an additional sink term is added to the momentum equation through specifying the pressure drop across the disk based on thrust coefficient concept. This drop of pressure is calculated from the following equation;

$$\Delta p = 0.5 \rho C_T U_{hub}^2 \tag{22}$$

To carry out the simulation, the complete set of the governing equations are solved by employing ANSYS FLUENT 15, in which the control-volume-based technique is used

for discretization. The SIMPLE algorithm is used for pressure velocity coupling and the first-order upwind scheme is used for all dependent variables. The inlet, wall, outlet boundary conditions and the additional source terms added to the governing equations are interpreted to the solver using User Defined Functions (UDF) programed in C - language.

RESULTS AND DISCUSSION

During the present study, two different test cases at different atmospheric conditions are simulated. The first one is the wind tunnel measurements conducted by Zhang et al. [4]. The model of wind turbine, used in that experiment, is 0.13 *m* diameter with a hub height of 0.105 *m* and it was operating under CBL condition. The second test case is the field measurements carried out at the Energy Research Center of Netherlands (ECN) test farm by Machielse et al. [32]. The wake measurements were recorded during SBL conditions, downstream a wind turbine with rotor diameter and hub height of 80 *m* each. For this case, two free stream inflow conditions are performed and compared with the available experimental data. Table 1 summaries the operating conditions used in the simulation for all test cases.

The numerical results of the adopted two methods using the standard k-ε, Crespo and El- Kasmi turbulence models are compared with the experimental data reported by Zhang et al. [4] in Figs. 3, 4 and 5. The compared data are obtained at a vertical center plane of the wake at distances 2, 3, 5 and 10 *D* downstream of the turbine.

Fig. 3 demonstrates the change of the normalized streamwise velocity u/U_{hub}, with the dimensionless vertical distance *z/D*. From this Figure, it can be depicted that, there is no significant difference between direct and indirect approaches at all downstream positions for the three turbulence models. In addition, overestimation of the streamwise velocity is observed at the near wake region up to *x/D* = 3, while there are good agreements with experimental data at *x/D*= 5 and 10. Introducing the dissipation term of El Kasmi model improves the wake prediction at the locations of 3 and 5 *D* downstream, as compared with the standard k-ε (Fig. 3a) and Crespo (Fig. 3b) models. However, it delays the wake recovery further downstream at x/*D* = 10, as noticed from Fig. 3c.

The distribution of the turbulence intensity ($TI = \sqrt{2k/3}/U_{hub}$) in the vertical direction through the wake is shown in Fig. 4. The numerical results obtained from both direct and indirect methods give also similar behavior, except a little deviation observed at the lower part of the wake. This deviation increases as the wake proceeds downstream with a little decrease in indirect method compared with direct one. Similar behavior was obtained by Abdelsalam et al. [33] for neutral ABL. In addition, the duel-peak pattern detected experimentally at *x/D*= 2, 3 and 5, is resulted from rotor tip vortices and high shear production of turbulent kinetic energy caused by strong velocity gradients at wake boundary, Zhang et al. [4]. This is not predicted by the numerical solution of the three turbulence models, which may be due to representing the turbine rotor with actuator disk instead of the actual rotor geometry. Overall, both of the two methods along with the three turbulence models underestimate the TI in the wake region although, good comparison with experimental data is experienced vertically far away

from the wake, starting approximately at *z/D* = 1.5. The linearity of all used turbulence models is the main reason for such deviations, see Balabel et al. [34].

The vertical distribution of the normalized kinematic shear stress $\overline{\acute{u}\acute{w}}/U_{hub}^2$ is shown in Fig. 5. At *x/D* = 2 and 3, a positive momentum flux is noticed in the lower part of the wake. Conversely, at the upper part of the wake, a negative momentum flux is observed, which is due to the momentum transport between the large momentum sink in the wake center and the ambient air. The standard k-ε turbulence model is the best among the adopted models to qualitatively predict the same trend of the experimental data using both methods. The use of model constant value of $C_\mu = 0.033$ instead of the standard value of $C_\mu = 0.09$, leads to a reduction in the turbulent viscosity according to Eq. (14), which in turn reduces mixing process of the wake with ambient flow. Hence, the kinematic shear stress becomes uniformly distributed along vertical direction near the wake center for Crespo and El Kasmi models. Moreover, the momentum flux approaches zero value at the inner core of the wake especially for El Kasmi model in the near wake region at *x/D* = 2 and 3. In the vertical direction far away from the wake region, it can be inferred that the mixing process vanishes and the momentum flux approaches zero. This may be due to the small vertical gradients of axial wind velocity in this region.

Because of the lack of temperature data for the ECN test case, indirect method is used to perform the numerical simulation of that case and to compare the achieved results with the experimental data of Machielse et al. [32]. Fig. 6 compares the numerical and experimental results of the axial velocity distribution u/U_{hub} for the inflow wind speed of $U_{hub} = 9.15\ m/s$ and turbulence intensity of $TI = 11.7\ \%$, prevailing at the hub height. It is seen from the figure that, El Kasmi model predicted well the wake velocity at x/*D* = 2.5, while, there is an overestimation of the wake deficit at x/*D* = 3.5. The other two turbulence models underestimate the wake deficit at the two positions. This can be attributed to the increase in the turbulent dissipation rate through the added dissipation term which in turn decreases the wake turbulent kinetic energy and delays the wake recovery.

On the other hand, the results of the turbulence intensity presented in Fig. 7 show that, Crespo model compares well with the experimental data, in comparison with standard k-ε and El Kasmi models. However, the double shoulder pattern of TI is captured only by El Kasmi model because of its well prediction of the velocity distribution at wake frontiers.

For the inflow conditions of $U_{hub} = 11.08\ m/s$ and $TI = 11.8\ \%$, the experimental data are only available for the wake velocity. It is seen from Fig 8 that, there is a good agreement between the results of El Kasmi model and the experimental data. There is an overestimation of the wake velocity using k-ε and Crespo models, as noticed also in the previous case.

CONCLUSIONS

In the present study, two different numerical techniques namely direct and indirect methods were applied to investigate the influence of the atmospheric stability on the wind turbine wake behavior. The turbine rotor was modeled using actuator disk approach. The standard k-ε model and another two modified models, known as Crespo

and El kasmi models were used for turbulence modeling. Approximately, there is no significant deviation between the numerical results of the direct and the indirect approaches, for the three turbulence models. Comparison of the present numerical prediction with the experimental data available for two test cases illustrated that, an overestimation of the wake velocity is featured at the near wake region especially when using the standard k-ε and Crespo models. Furthermore, an underestimation of the turbulence quantities is achieved when using the three adopted turbulence models. A general conclusion that can be drawn from the present work is that, using indirect model combined with El Kasmi turbulence closure gives satisfactory results compared with the reported experimental data. However, further validation with experimental data is required to better understand the physical mechanism of the interaction between the wind turbine wakes (small scale turbulence) and the ABL (large scale turbulence).

REFERENCES

[1] G.P. Van den Berg, "Wind turbine power and sound in relation to atmospheric stability", Wind Energy, Vol. 11, pp. 151-169 (2008).

[2] S. Wharton and J. K. Lundquist, "Atmospheric Stability Impacts on Power Curves of Tall Wind Turbines – An Analysis of a West Coast North American Wind Farm", LLNL-TR-424425 (2010).

[3] L. P. Chamorro and F. Porté-Agel, "Effects of Thermal Stability and Incoming Boundary-Layer Flow Characteristics on Wind-Turbine Wakes: A Wind-Tunnel Study", Boundary-Layer Meteorol., Vol. 136, pp. 515-533 (2010).

[4] W. Zhang, C. D. Markfort, and F. Porté-Agel, "Wind-turbine wakes in a convective boundary layer: A wind-tunnel study", Boundary-Layer Meteorol., Vol. 146, pp. 161-179 (2013).

[5] P. E. Hancock and F. Pascheke, "Wind-tunnel simulation of the wake of a large wind turbine in a stable boundary layer: Part 2, the wake flow", Boundary-Layer Meteorol., Vol. 151, pp. 23-37 (2014).

[6] R. W. Baker and S. N. Walker, "Wake measurements behind a large horizontal axis wind turbine generator", Solar Energy, Vol. 33, No. 1, pp. 5-12 (1984).

[7] M. Magnusson and A. S. Smedman, "Influence of atmospheric stability on wind turbine wakes", Wind Energy., Vol. 18, pp. 139-152 (1994).

[8] G. V. Iungo and F. Porté-Agel, "Volumetric lidar scanning of wind turbine wakes under convective and neutral atmospheric stability regimes", J. Atmos. Oceanic Technol., Vol. 31, No. 10, pp. 2035-2048 (2014).

[9] M. Magnusson and A. S. Smedman, "Air flow behind wind turbines", J. Wind Eng. Ind. Aerodyn., Vol. 80, pp. 169-189 (1999).

[10] A. Crespo and J. Hernandez, "Turbulence characteristics in wind-turbine wakes", J. Wind Eng. Ind. Aerodyn., Vol. 61, pp. 71-85 (1996).

[11] A. El Kasmi and C. Masson, "An extended k-ε model for turbulent flow through horizontal axis wind turbines", J. Wind Eng. Ind. Aerodyn., Vol. 96, pp. 96-103 (2008).

[12] K. G. Rados, J. M. Prospathopoulos, N.Ch. Stefanatos, E.S. Politis, P.K. Chaviaropoulos and A. Zervos, "CFD modeling issues of wind turbine wakes under stable atmospheric conditions", European Wind Energy Conference and Exhibition, Marseille (2009).

[13] B. Sanderse, S. P. van der Pijl2 and B. Koren2, "Review of computational fluid dynamics for wind turbine wake aerodynamics", Wind Energy, Vol. 14, pp. 96-103 (2011).
[14] J. M. Prospathopoulos, E. S. Politis, K. G. Rados and P. K. Chaviaropoulos, "Evaluation of the effects of turbulence model enhancements on wind turbine wake predictions", Wind Energy, Vol. 14, pp. 285-300 (2011).
[15] M. J. Churchfield, S. Lee, J. Michalakes, and P. J. Moriarty, "A numerical study of the effects of atmospheric and wake turbulence on wind turbine dynamics", Journal of Turbulence, Vol. 13, No. 14, pp. 1-32 (2012).
[16] R. E. Keck, M. Mare, J. M. Churchfield, S. Lee, and G. Larsen, "On atmospheric stability in the dynamic wake meandering model", Wind Energy, Vol. 17, pp. 1689-1710 (2014).
[17] M. Bastankhah and F. Porté-Agel, "A new analytical model for wind-turbine wakes", Renewable Energy, Vol. 70, pp. 116-123 (2014).
[18] Y. T. Wu and F. Porté-Agel, "Large-eddy simulation of wind-turbine wakes: Evaluation of turbine parametrisations", Boundary-Layer Meteorol., Vol. 132, pp. 129-149 (2011).
[19] Y. T. Wu and F. Porté-Agel, "Atmospheric turbulence effects on wind-turbine wakes: An LES study", Energies, Vol. 5, No, 12, pp. 5340–5362 (2012).
[20] M. Abkar and F. Porté-Agel, "Influence of atmospheric stability on wind-turbine wakes: A large-eddy simulation study", Phys. Fluids, Vol. 27, No, 3, pp. 1–19 (2015).
[21] B. E. Launder and D. Spalding, "The numerical computation of turbulent flows", Comput. Methods Appl. Mech. Eng., Vol. 3, pp. 269-289 (1974).
[22] A. Crespo, F. Manuel, D. Moreno, E. Fraga and J. Hernandez, "Numerical analysis of wind turbine wakes", In: Proceedings of Delphi Workshop on Wind Energy Applications, Delphi, Greece, pp. 15-25 (1985).
[23] S. P. Arya, "Micrometeorology and Atmospheric Boundary Layer", Pure and Applied Geophysics, Vol. 162, pp. 1721–1745 (2005).
[24] C. Alinot and C. Masson, "k-ε Model for the Atmospheric Boundary Layer Under Various Thermal Stratifications", Journal of Solar Energy Engineering, Vol. 127, pp. 438–443 (2005).
[25] Roland B. Stull, "An Introduction to Boundary Layer Meteorology", Kluwer Academic Publishers, Dordrecht, (1988).
[26] W. P. Jones and B. E. Launder, "The Prediction of Laminarization with a Two-Equation Model of Turbulence", Int. J. Heat Mass Transfer, Vol. 15, pp. 301-314 (1972).
[27] "ANSYS FLUENT Theory Guide", pp. 59-60.
[28] Y. S. Chen and S. W. Kim, "Computation of turbulent flow using an extended k-ε turbulence closure model", NASA Contractor Report, NASA CR-179204 (1987).
[29] D. D. Apsley and I. P. Castro, "A Limited-Length-Scale k-ε Model for Neutral and Stably-Stratified Atmospheric Boundary Layer", Boundary-Layer Meteorol., Vol. 83, pp. 75-98 (1997).
[30] R. Howell, N. Qin, J. Edwards and N. Durrani, "Wind tunnel and numerical study of a small vertical axis wind turbine", Renewable Energy., Vol. 35, pp. 412-422 (2010).
[31] A. Parente, C. Gorle, J. van Beeck and C. Benocci, "Improved k-ε model and wall function formulation for the RANS simulation of ABL flows", J. Wind Eng. Ind. Aerodyn., Vol. 99, pp. 267-278 (2011).

[32] L.A.H. Machielse, P.J. Eecen, H. Korterink, S.P. van der Pijland and J.G. Schepers, "ECN test farm measurements for validation of wake models", European Wind Energy Conference & Exhibition, Milan, Italy., (2007).

[33] Ali M. Abdelsalam, K. Boopathi, S. Gomathinayagam, S.S. Hari Krishnan Kumar and Velraj Ramalingam, "Experimental and numerical studies on the wake behavior of a horizontal axis wind turbine", J. Wind Eng. Ind. Aerodyn., Vol. 128, pp. 54-65 (2014).

[34] A. Balabel and W. A. El-Askary, "On the performance of linear and nonlinear k-ε turbulence models in various jet flow applications", European Journal of Mechanics B/Fluids, Vol. 30, pp. 325-340 (2011).

Table 1. Operating conditions of the simulated test cases.

Test case	U_{hub} (*m/s*)	TI_{hub} (%)	u_* (*m/s*)	T_* (*K*)	T_w (*K*)	C_T (-)	z_0 (*mm*)	L (*m*)
Zhang et al. [4]	2.5	7.9	0.14	- 2.78	345	0.42	0.026	- 0.44
Machielse et al.[32]	9.15	11.7	0.38	-	-	0.76	17	365
	11.08	11.8	0.48	-	-	0.63	18	440

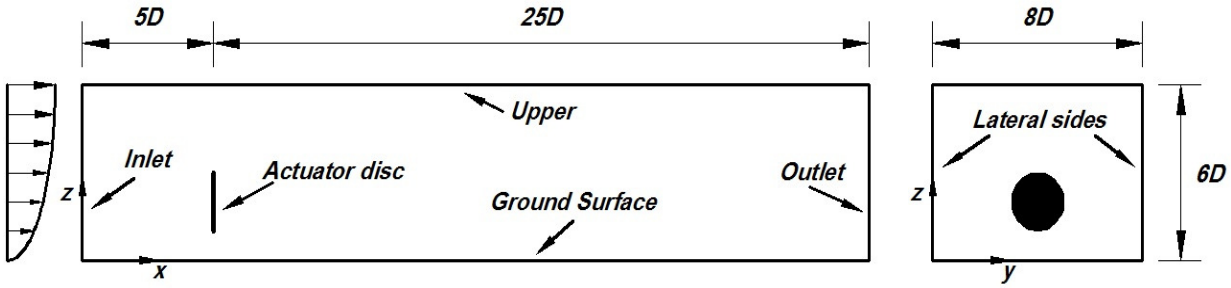

(a) Front view **(b)** Side view

Fig. 1. Schematic representation of the computational domain.

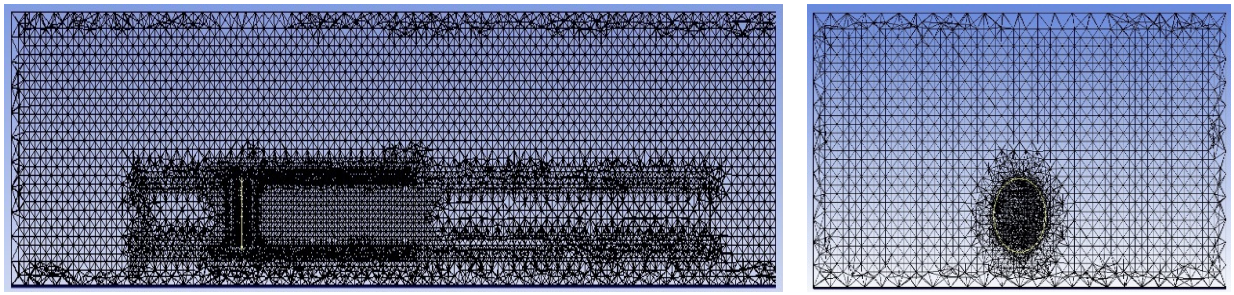

(a) Front view **(b)** Side view

Fig. 2. The computational grid at a vertical center plane across the actuator disk.

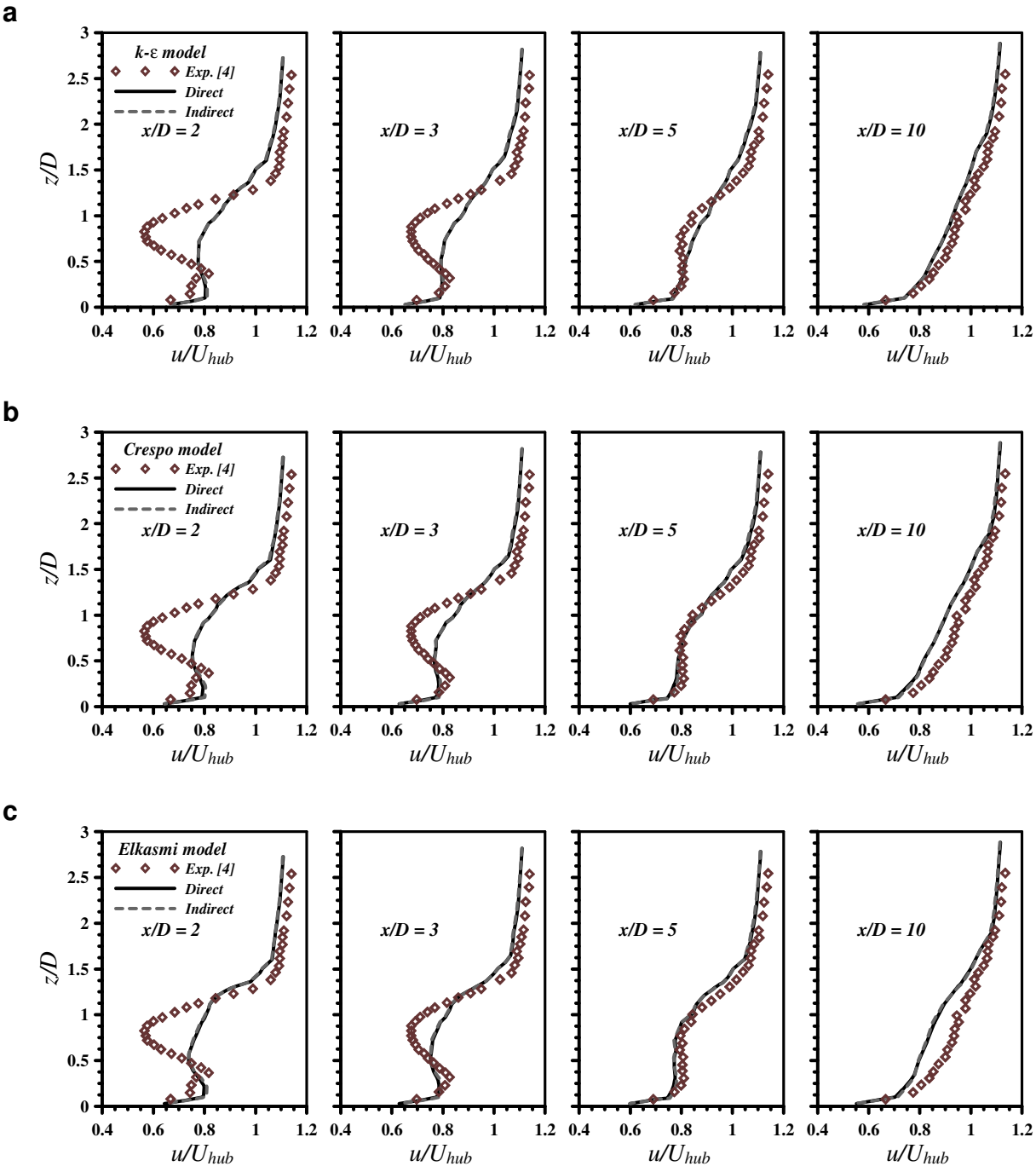

Fig. 3. Vertical distribution of the normalized streamwise wake velocity for Zhang et al. [4] test case, (a) Standard k-ε model, (b) Crespo model, and (c) El Kasmi model.

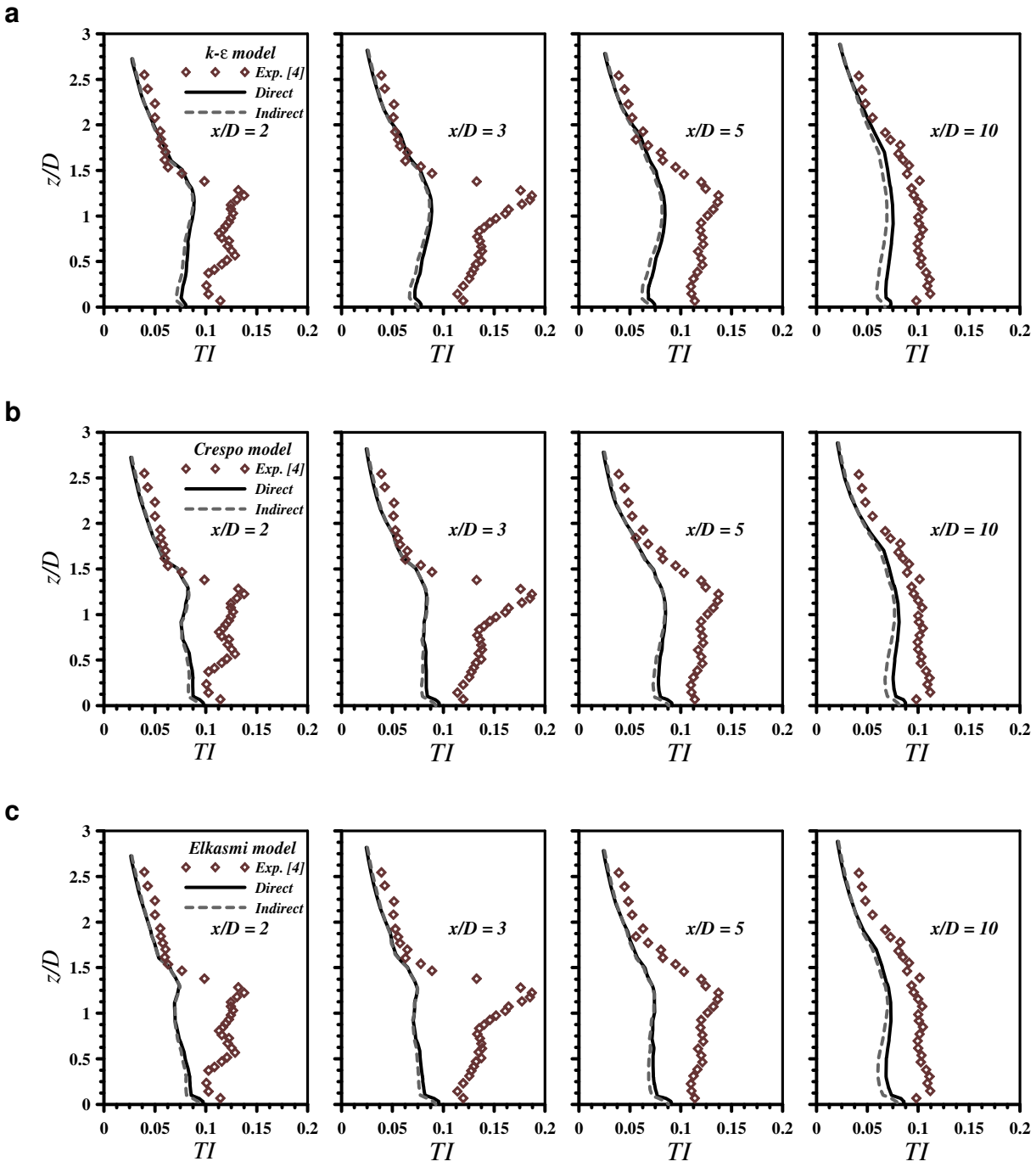

Fig. 4. Vertical distribution of the wake turbulence intensity for Zhang et al. [4] test case, (a) Standard k-ε model, (b) Crespo model, and (c) El Kasmi model.

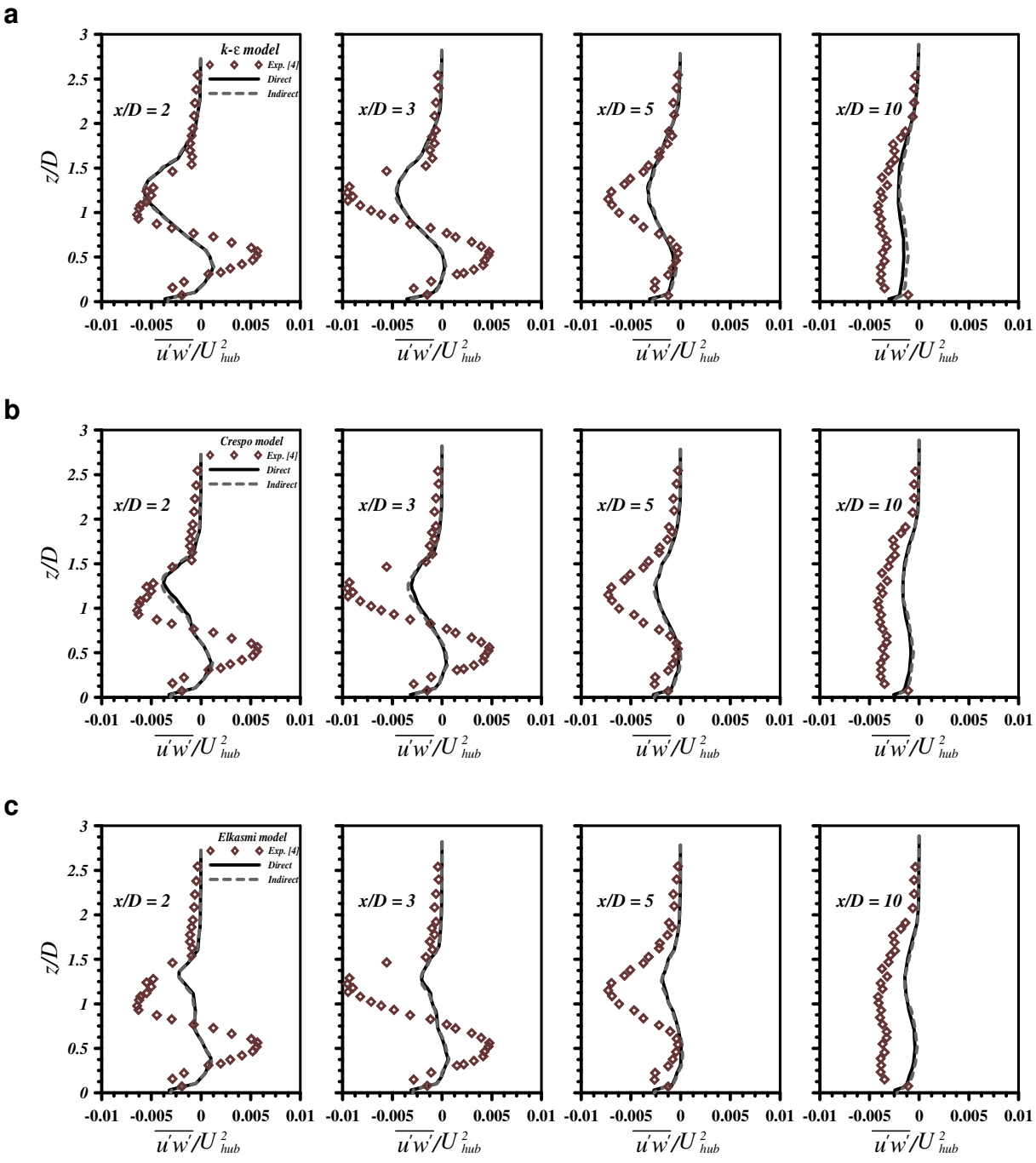

Fig. 5. Vertical distribution of the wake kinematic shear stress for Zhang et al. [4] test case, (a) Standard k-ε model, (b) Crespo model, and (c) El Kasmi model

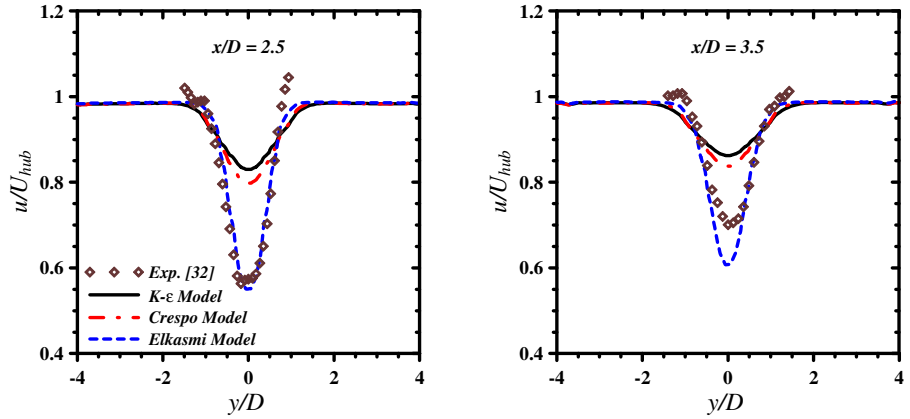

Fig. 6. Wake velocity distribution for the ECN test case, Machielse et al. [32] ($U_{hub} = 9.15\ m/s$ and $TI = 11.7\ \%$)

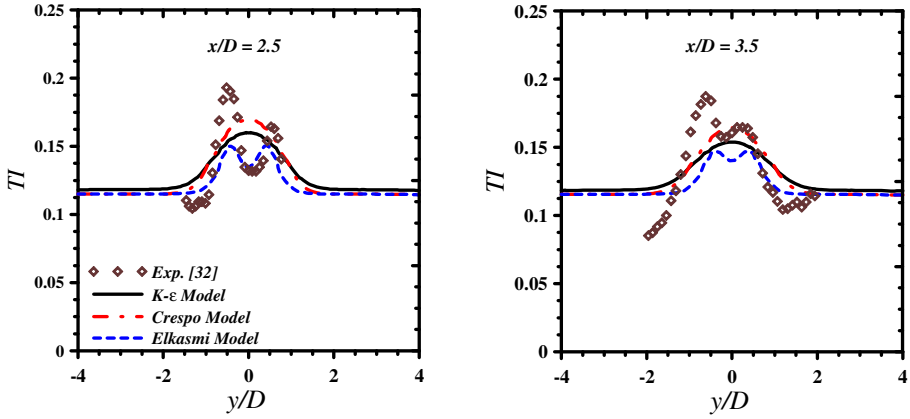

Fig. 7. Wake turbulence intensity for the ECN test case, Machielse et al. [32] ($U_{hub} = 9.15\ m/s$ and $TI = 11.7\ \%$)

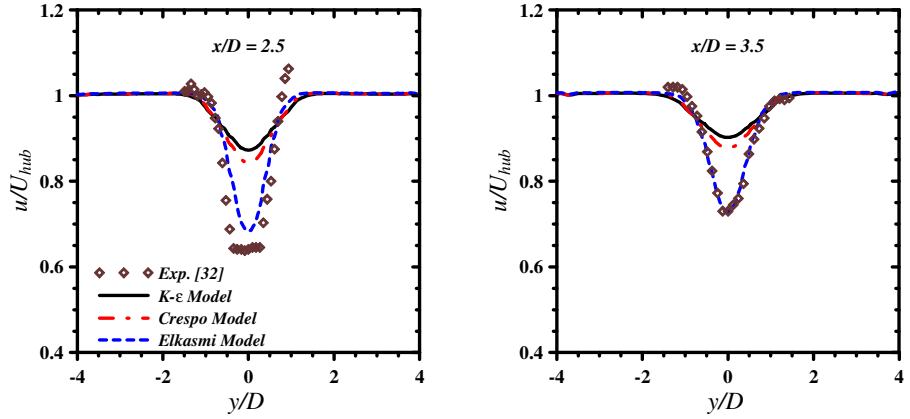

Fig. 8. Wake velocity distribution for the ECN test case, Machielse et al. [32] ($U_{hub} = 11.08\ m/s$ and $TI = 11.8\ \%$)